

# Satellite edge computing for real-time and very-high resolution Earth observation

Israel Leyva-Mayorga, *Member, IEEE*, Marc M. Gost, Marco Moretti, Ana Pérez-Neira, *Fellow, IEEE*, Miguel Ángel Vázquez, Petar Popovski, *Fellow, IEEE*, and Beatriz Soret, *Senior Member, IEEE*

## Abstract

In real-time and high-resolution Earth observation imagery, Low Earth Orbit (LEO) satellites capture images that are subsequently transmitted to ground to create an updated map of an area of interest. Such maps provide valuable information for meteorology or environmental monitoring, but can also be employed in near-real time operation for disaster detection, identification, and management. However, the amount of data generated by these applications can easily exceed the communication capabilities of LEO satellites, leading to congestion and packet dropping. To avoid these problems, the Inter-Satellite Links (ISLs) can be used to distribute the data among the satellites for processing. In this paper, we address an energy minimization problem based on a general satellite mobile edge computing (SMEC) framework for real-time and very-high resolution Earth observation. Our results illustrate that the optimal allocation of data and selection of the compression parameters increase the amount of images that the system can support by a factor of 12 when compared to directly downloading the data. Further, energy savings greater than 11% were observed in a real-life scenario of imaging a volcanic island, while a sensitivity analysis of the image acquisition process demonstrates that potential energy savings can be as high as 92%.

Israel Leyva-Mayorga and Petar Popovski are with the Department of Electronic Systems, Aalborg University, 9220 Aalborg, Denmark (e-mail: {ilm, petarp}@es.aau.dk). Marc M. Gost is with the Centre Tecnològic de Telecomunicacions de Catalunya and the Dept. of Signal Theory and Communications, Universitat Politècnica de Catalunya, Spain (email: marc.martinez.gost@upc.edu). Marco Moretti is with the Dept. of Information Engineering, University of Pisa, Italy (email: marco.moretti@unipi.it). Ana Pérez-Neira is with ICREA, the Centre Tecnològic de Telecomunicacions de Catalunya and the Dept. of Signal Theory and Communications, Universitat Politècnica de Catalunya, Spain (email: ana.perez@cttc.es). Miguel Ángel Vázquez is with the Centre Tecnològic de Telecomunicacions de Catalunya, Spain (email: mavazquez@cttc.cat). Beatriz Soret is with the Dept. of Communications Engineering, University of Málaga, Spain and with the Department of Electronic Systems, Aalborg University, 9220 Aalborg, Denmark (email: bsoret@ic.uma.es).

This work was partially funded by SatNEx-V, co-funded by the European Space Agency (ESA). The work of Ana Pérez-Neira is partially supported by Project IRENE- (PID2020-115323RB-C31) funded by MCIN/AEI/ 10.13039/501100011033.

## I. INTRODUCTION

Satellites in LEO are widely used for Earth observation purposes as they can construct high-resolution maps of large areas by capturing images from space as they orbit the Earth. These maps can be used in various applications, as in meteorology, agriculture, or environmental monitoring [1]. They are also very valuable in near-real time applications, such as disaster detection and identification, supporting the coordination of the emergency response. Due to the limited storage in the individual LEO satellites, the images must be 1) captured, 2) processed for compression and/or optical correction, and 3) transmitted to ground for storage and/or distribution across the terrestrial infrastructure.

The area covered by each individual satellite image depends on numerous factors. Namely, the field of view (FoV) of the instrument/camera is the angle that determines the observable space of the camera sensor. The FoV together with the altitude of deployment of the satellite determine the *swath*, which is the width of the observable area on the surface of the Earth. Then, the swath and the resolution of the instrument/camera determine the ground sample distance (GSD), which is the distance covered by each single pixel. As an example, the European Space Agency (ESA) Sentinel-2 mission is located at an altitude of 748 km and captures images in the visible spectrum with a GSD of 1.5 m [2]. In total, the swath for Sentinel-2's visible spectrum instrument is only 60 km. Other common values for the GSD are in the range between 0.3 and 3 meters [3], [4].

To achieve a high image resolution, the GSD must be small and, in turn, so does the area covered by a single image. For example, the area covered by an image in high-definition (HD) format with a GSD of 3 m is around  $18 \text{ km}^2$ , which is smaller than several European airports. Therefore, high-resolution maps of large areas must be created by capturing and organizing a large number of images. These images must be captured with a sufficiently high frequency to avoid coverage holes in the map.

Traditionally, the Earth observation satellites would communicate directly with a ground station (GS) to download the collected data. However, this greatly limits the amount of data that can be collected. In contrast, modern Earth observation missions possess numerous satellites with advanced communications and processing capabilities. For instance, recent advances in free-space optical (FSO) communications technology [5], in combination with the stable relative positions of satellites in the same orbital plane, make it possible to establish intra-plane ISLs to connect neighboring satellites in the same orbital plane using high-data rate FSO links. Such links can

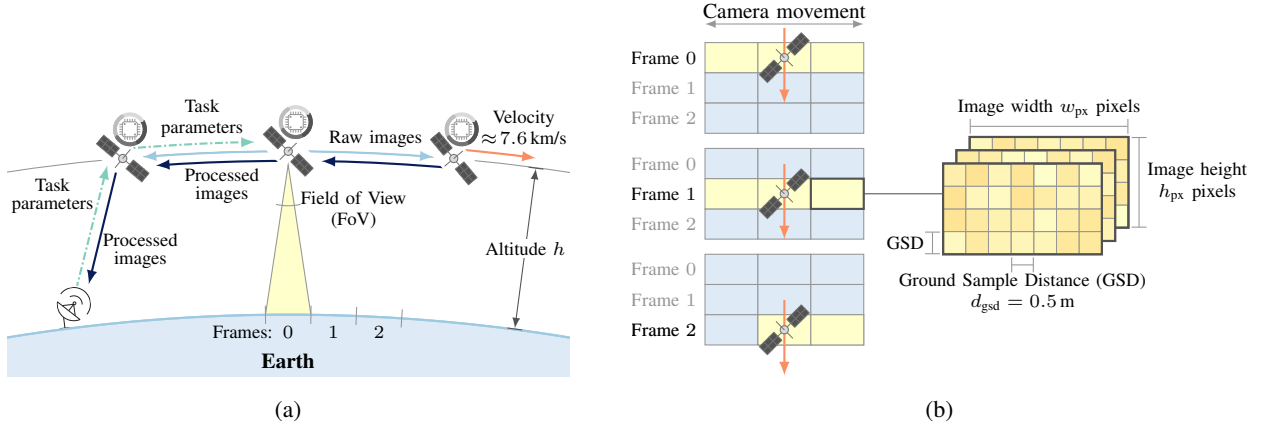


Fig. 1. Earth observation application where a satellite scans the area of interest. (a) The FoV and the altitude of the satellites determine the area covered by each image. The raw images can be shared with the nearby satellites to process them in a distributed manner and, then, send them to the GS. (b) The satellite captures a frame, consisting of  $W_k$  images, at slot  $k$  as indicated by the yellow area. The value of  $W_k$  may be different for each  $k$  depending on the dimensions of the area of interest.

be used to distribute the images across the neighboring satellites, forming a SMEC cluster with distributed processing capabilities.

Fig. 1 illustrates an Earth observation mission relying on a SMEC cluster to distribute the data to be processed and compressed by multiple satellites before being downloaded to the GS. As it can be seen, the orbital velocity of the satellite creates the need to capture images frequently to avoid coverage holes and the frequency is determined by the FoV and the altitude of the satellite. Specifically, the maximum period at which the images must be captured to avoid coverage holes is called the ground track frame period (GTFP), which imposes the timing constraints in the satellite processing and communication subsystems. In such setup, illustrated in Fig. 1b, the system operation can be divided into time slots. At each time slot, the satellite scans the area of interest by capturing a set of side-by-side images called a frame. Then, to maintain the stability in the processing and communication subsystems at the satellites, the time needed for processing and for communication at each link must be lower than that of the duration of a time slot. This is the scenario of interest for the present paper.

The generation of enormous amounts of data in Earth observation applications is a common concern, especially regarding the downlink capacity (i.e., satellite-to-ground link). Therefore, two main approaches have been formulated to reduce the amount of data to be delivered: early discard [3], [4] and compression [6]. Early discard of images with relatively low information

content (e.g., cloud coverage) effectively reduces the amount of data transmitted to ground [3], [4]. Note that the efficiency of early discard is mostly based on autonomous decisions at the satellites, which determine which images to transmit to ground and which ones to discard. Even though this inference process can be enhanced with techniques such as image-chain simulation (ICS) to evaluate the quality of the captured images [7], it may be problematic for mission-critical applications, for example, emergency scenarios, where partially obstructed images can still be valuable for the GS. To avoid these problems, the satellites might instead simply execute an algorithm to compress the collected data. In our previous work [6], we focused on an Earth observation scenario with power allocation for communication and where the source satellite was allowed to choose between directly downloading the data or compressing it locally. Since the satellites rely on solar panels and rechargeable batteries for energy supply, the optimization objective was to minimize the energy consumption.

While the literature on SMEC for Earth observation focuses on local processing of the data, there are numerous examples of terrestrial mobile edge computing (MEC) and SMEC that consider the optimization of distributed processing, which is a generalization of local processing. For example, lossless compression was considered to occur both at the source mobile device and at the edge server in a terrestrial MEC to reach a combined compression ratio [8]. In a similar fashion, the benefits of offloading computation tasks from mobile users in remote areas to a SMEC network were studied in [9]. The main contribution of this latter paper, which builds on recent literature on SMEC architectures [10]–[13], is to propose a three-tier scheme where the tasks with low computational complexity are directly processed at the mobile users and the rest are distributed either to a ground cloud or to the satellite edge. This complex allocation problem is solved with the alternating direction method of multipliers (ADMM). Nevertheless, most of the literature on SMEC, with a few clear exceptions [3], [4] that include our previous work [6], deals with tasks generated at the mobile users and, hence, mimics the traditional functionality of a terrestrial MEC that now includes satellites.

The present paper represents a major extension of our previous work and a major deviation with respect to the SMEC literature described above by considering real-time high-resolution Earth observation applications where the real-time requirements are defined by the dynamics of the system. In the considered scenario, the source satellite, denoted as  $v_0$ , captures frame at each time slot  $k \in \{1, 2, \dots, K\}$ , where  $K$  is the total number of frames in the task and the satellites in an orbital plane communicate through high-data rate FSO ISLs. Given that the images, and

hence, the frames can be processed locally or in a distributed manner by dividing the data in each frame into segments, the GS defines the task parameters, including the satellites in the SMEC cluster, based on the predictable movement of the satellites. In the following, we describe a general SMEC framework for real-time and very-high resolution Earth observation, which is based on classical communication models for distributed processing architectures, but considers the distinctive characteristics of LEO satellite communications, such as limited bandwidth and links with heterogeneous capacity.

- 1) *Segmentation*: At each time slot  $k \in \{1, 2, \dots, K\}$ , the source satellite  $v_0$  captures a frame  $k$  with  $W_k$  images for a total size  $D_k$  bits and divides it into segments.
- 2) *Allocation*: Each of the satellites in the SMEC cluster for frame  $k$ , namely  $n \in \mathcal{N}_k$ , will receive a segment, which is a fraction  $x_k^{(n)}$  of the total amount of data in the frame. The GS might also indicate a fraction of the frame  $x_k^{(g)}$  that will not be processed by the satellites but downloaded directly without processing.
- 3) *Scatter*: The source satellite distributes the segments to all the satellites in the SMEC cluster  $n \in \mathcal{N}_k$  using high-data rate ISLs. The rest of the data are routed directly to the GS without processing.
- 4) *Distributed processing*: The segments are processed at the satellites, with a consequent reduction in the size of the data by a factor  $\rho_k$ , called the compression ratio. Hence, the resulting size of the segment processed by satellite  $n$  is  $x_k^{(n)}/\rho_k$ . The CPU frequency selected to process the  $k$ -th frame at satellite  $n$  is denoted as  $f_k^{(n)}$ .
- 5) *Gather*: Once processing is completed, the satellites in the SMEC cluster  $\mathcal{N}_k$  send the processed segments to the GS through the destination satellite  $v_d$ .

Building on the described SMEC framework, Fig. 2 illustrates the diverse options for executing a task with the GTFP as real-time constraint. The data can be directly downloaded to the GS, but this requires a large amount of transmission time in both the satellite-to-GS and ISL, which may cause backlog in the communication links. On the other hand, the data can be processed locally, at the source satellite, but this might incur in a large processing latency due to the limited processing power, which may cause backlog at the CPU of the source satellite. Finally, the data can be distributed across a SMEC with 4 satellites, which alleviates the load in both the communication links and at the individual CPUs and allows to reduce the communication at each individual link and the processing at each CPU so that the real-time constraint, defined

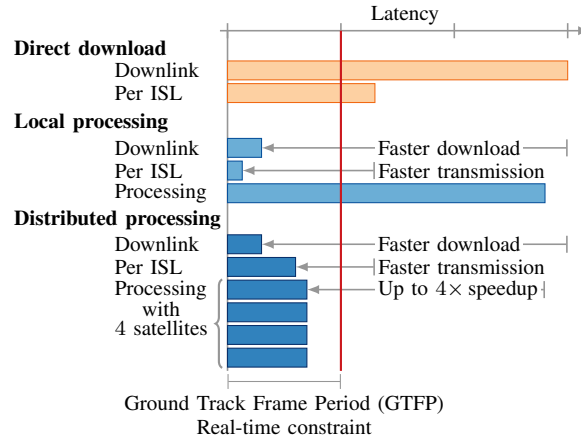


Fig. 2. Illustration of the different options for data delivery in high-resolution Earth observation: direct download, local processing, and distributed processing.

by the GTFP, is fulfilled, which guarantees the stability of the communication and processing subsystems.

The main contribution of this paper are described in the following.

- 1) We define a novel and general model for high-resolution Earth observation imagery, along with its real-time constraints imposed by the physical (i.e., orbital) parameters of LEO constellations and of the imaging instruments.
- 2) We formulate and solve a global optimization problem for the segmentation, scatter, processing, and gather phases of our general SMEC framework. Given that the satellites have a limited battery supply, the objective of distributing the tasks across the satellites in the constellation is to minimize the overall energy consumption while fulfilling the limitations of the processing frequency at the satellites' CPU, and the rates at the ISLs and satellite-to-ground link.
- 3) We evaluate the performance of the proposed framework in several baseline scenarios but also in a real-life scenario of scanning the island of La Palma.

In the baseline scenarios, our results illustrate that the number of images that can be transmitted to the GS with our SMEC approach is up to  $12\times$  larger when compared to direct download without processing and up to  $200\times$  larger when compared to processing only at the source satellite. Furthermore, the energy consumption of our SMEC approach is up to  $10\times$  lower than with direct download. Furthermore, when compared to optimizing each frame independently,

jointly optimizing the task parameters for the  $K$  frames leads to energy savings of up to 92% in the baseline scenarios, which have a relatively low number of images per frame. In the real-life scenario, where the satellites are in charge of scanning the island of La Palma, our results show that the energy consumption can be reduced at up to 11% by optimizing the task parameters for the  $K = 82$  frames when compared to optimizing for each frame independently.

The rest of the paper is organized as follows. Section II describes the system model. Next, the optimization problem is formulated in Section III, numerical results are presented in Section IV, and concluding remarks are given in Section V.

## II. SYSTEM MODEL

### A. Framing

We consider an orbital plane (i.e., ring) in a LEO satellite constellation and a GS  $g$ . The orbital ring is comprised of  $N$  satellites uniformly spaced along the orbit and deployed at an altitude  $h$  km above the Earth's surface. The satellites possess, among other subsystems, a camera, a processing payload, and communication modules to establish a radio frequency link towards the GS as well as high-data rate FSO ISLs with the two neighboring satellites. Hence, the satellites in the orbital plane form a ring topology.

The satellites in the orbital plane serve an Earth observation application with pre-planned tasks. Each task involves capturing images to scan a specific area of interest, which must be transmitted to the GS. The camera is used to capture images of a fixed size

$$D_{\text{img}} = w_{\text{px}} h_{\text{px}} q_{\text{px}} \text{ bits}, \quad (1)$$

where  $w_{\text{px}}$  and  $h_{\text{px}}$  are the width and height in pixels and  $q_{\text{px}}$  is the number of bits to represent each pixel. Throughout this article, we assume that  $h_{\text{px}} < w_{\text{px}}$  is aligned with the velocity vector of the satellite (i.e., the roll axis). The satellites capture images by pointing directly towards the Earth and by rotating the camera perpendicularly to the velocity vector as illustrated in Fig. 2. Therefore, the satellite itself must enter the area of interest to start capturing the images.

The average distance between adjacent pixel centers  $d_{\text{gsd}}$  taken when pointing directly at the nadir point is called the GSD, which is a function of  $w_{\text{px}}$ , the FoV, and the satellite altitude  $h$  [3]. The area covered by a single image is

$$A \approx w_{\text{px}} h_{\text{px}} d_{\text{gsd}}^2 \quad (2)$$

TABLE I  
PARAMETERS DEFINED IN THE SYSTEM MODEL

Symbol	Description
<b>Orbital plane</b>	
$N$	Number of satellites in the orbital plane
$h$	Altitude of deployment of the satellites [m]
$h_{\text{px}}$	Height of each image [pixels]
$w_{\text{px}}$	Width of each image [pixels]
$q_{\text{px}}$	Amount of bits per pixel
$D_{\text{img}}$	Size of each image [bits]
$W_k$	Number of side-by-side images in frame $k$
$d_{\text{gsd}}$	Average ground sampling distance [m]
$T_{\text{GTF}}(h_{\text{px}}, d_{\text{gsd}}, h)$	Ground track frame period (GTFP) [s]
<b>Processing</b>	
$f_{\text{CPU}}$	Highest CPU frequency [Hz]
$f_k^{(n)}$	CPU frequency [Hz] for processing at satellite $n$ and frame $k$
$N_{\text{CPU}}$	Number of available processing cores per satellite
$\rho_k$	Compression ratio for frame $k$
$\epsilon$	Parameter that depends on the compression algorithm
$C(\rho_k, \epsilon)$	Number of CPU cycles to compress one bit of data
<b>Communication</b>	
$R_k$	Data rate to transmit frame $k$ to the GS [bps]
$P_{\text{tx}}$	Transmission power [W]
$R_{\text{ISL}}$	Fixed data rate at the ISLs [bps]
$P_{\text{ISL}}$	Fixed transmission power at the ISLs [W]
$\eta$	Fraction of power consumed during transmission at the ISLs above normal operation
<b>Segment allocation</b>	
$X \in \mathbb{Z}^{K,N}$	Segment allocation matrix [bits]
$\mathbf{x}_k \in \{0, 1, \dots, D_k\}^N$	Segment allocation vector for frame $k$ [bits]
$x_k^{(n)} \in \{0, 1, \dots, D_k\}$	Segment allocation for satellite $n$ and frame $k$ [bits]

and the vertical distance–aligned with the roll axis of the satellite–covered is  $h_{\text{px}}d_{\text{gsd}}$  m.

The task and, similarly, the operation of the system are divided into  $K$  time slots of duration equal to the GTFP. At each time slot  $k$ , the source satellite  $v_0$  captures a frame comprised of  $W_k \in \mathbb{N}^+$  side-by-side images by rotating the camera perpendicularly to its velocity vector to cover the area of interest as it moves. The number of images  $W_k$  can be different for each frame



in a task as exemplified in Fig. 1b, where frame  $W_0 = W_1 = 3$  images and  $W_2 = 2$ .

We assume that the time to capture the  $W_k$  images in a frame and to make them available for the processing algorithm and the communication modules (i.e., to write the data in memory) does not impact the real-time constraints of the system. The resulting size of the  $k$ -th frame is  $D_k = W_k D_{\text{img}}$  bits and the frame is approximately  $W_k w_{\text{px}} d_{\text{gsd}}$  meters wide.

Capturing frames at exactly the GTFP ensures that there are no coverage gaps, but also that there are no two pixels that cover the same area in two consecutive frames taken by the same satellite. To calculate the GTFP, let  $T_o(h)$  be the orbital period of a satellite deployed at altitude  $h$ . Then,  $T_o(h)$  can be closely approximated as

$$T_o(h) \approx \sqrt{\left(\frac{4\pi^2}{GM_E}\right) (R_E + h)^3}, \quad (3)$$

where  $G$  is the universal gravitational constant;  $M_E$  and  $R_E$  are the mass and radius of the Earth, respectively. The GTFP, denoted as  $T_{\text{GTF}}$ , is given as

$$T_{\text{GTF}}(h_{\text{px}}, d_{\text{gsd}}, h) = \frac{h_{\text{px}} d_{\text{gsd}} T_o(h)}{2\pi R_E}. \quad (4)$$

Without loss of generality, we define  $t_k = kT_{\text{GTF}}$  as the time when frame  $k$  is captured by the satellite. Consequently,  $t_0 = 0$ .

The frames may be processed before they are sent to ground, which involves, for example, correction of optical anomalies, compression, and encoding. Specifically, a frame captured by a satellite  $v_0$ , the source, can be processed either locally or in a distributed manner to reduce its size by a compression factor  $\rho > 1$ , such that the resulting size of the frame is  $D_k/\rho$ .

### B. Compression

Let  $C(\rho_k, \epsilon)$  be the complexity of the compression algorithm, defined as the number of CPU cycles to compress one bit of data by a compression ratio  $\rho_k$ , being  $\epsilon$  a positive constant that depends on the compression algorithm. In traditional and pure JPEG compression, the complexity can be considered as constant w.r.t. the compression ratio  $\rho_k$  since the latter is only determined by the entries of the quantization matrix, which does not affect the number of operations to be performed. Nevertheless, setting a constant compression complexity might only represent a small subset of possible compression algorithms.

Instead, we adopt a model where the complexity of the compression algorithm increases exponentially with the compression ratio as  $C(\rho_k, \epsilon) = e^{\epsilon\rho_k} - e^\epsilon$  [14]. This latter model covers

several popular compression techniques, such as Zlib, Zstandard, and XZ compression and makes our optimization framework more general. Consequently, by selecting the exponential model for the complexity of the compression algorithm, our framework is applicable to a much wider range of compression algorithms than the constant complexity model for JPEG. Furthermore, as it will be seen in Section III, adoption of the exponential model creates a trade-off between the energy used for processing and for communication. In contrast, selecting the optimal compression ratio under a constant complexity model for the formulated optimization problem would be trivial.

To process and compress the images, the processing payload of the satellites consists of a CPU with  $N_{\text{CPU}}$  cores and a maximum clock frequency  $f_{\text{CPU}}$ . The satellites are able to adapt the CPU clock frequency for each frame  $k \in \mathcal{K}$  in the task through Dynamic Voltage and Frequency Scaling (DVFS), which allows to reduce the energy consumption of tasks with relaxed latency requirements. Therefore, we define  $f_k^{(n)}$  as the CPU clock frequency selected by satellite  $n \in \mathcal{N}$  to process the data belonging to frame  $k$ .

Let  $T_k^{\text{proc}}$  be the execution time of the image processing algorithm for a frame in task  $k$ , which is given, for satellite  $n$ , as

$$T_k^{\text{proc}}(n, D_k, \rho, f_k; \epsilon, N_{\text{CPU}}) = \frac{D_k C(\rho, \epsilon)}{N_{\text{CPU}} f_k^{(n)}}. \quad (5)$$

The processing of the data received by the satellites is managed by a scheduler that operates in a first-in first-out fashion. Hence, it may need to queue the processing of a segment until the processing of the previous one is completed and the CPU is available. Specifically, we denote the queueing time to process the data received at time  $t$  at satellite  $n$  as  $Q_t^{\text{proc}}(n) \in \mathbb{R}^+$  seconds. In other words, the data received at time  $t$  must wait in the queue of satellite  $n$  until time  $t + Q_t^{\text{proc}}(n)$  before it can be processed. Throughout this paper, we focus on maintaining the stability of the processing queues rather than on their impact on the overall latency.

### C. Communication

After processing, the resulting data must be transmitted to the GS  $g$ . The communication modules are used to establish communication with the satellites in the same orbital plane via the intra-plane ISLs, and with  $g$ . Specifically, intra-plane ISLs are established with the two neighboring satellites in the same orbital plane and a downlink satellite-to-ground link is established between  $g$  and the closest satellite. Let  $\mathcal{G}_k = (\mathcal{V}, \mathcal{E}_k)$  be the directed graph that represents the system at time  $t_k$ , where  $\mathcal{V} = \mathcal{N} \cup \{g\}$  is the vertex set and  $\mathcal{E}_k$  is the edge set

at time  $t_k$ . As mentioned above, we consider a time-slotted system and, hence, update graph  $\mathcal{G}_k$  along with its parameters by taking a snapshot at the beginning of each time slot.

Without loss of generality, we denote the source satellite as  $v_0$  and the destination satellite, which has a direct connection to the GS, as  $v_d$ . The directed edges  $(u, v) \in \mathcal{E}_k$  represent the full-duplex communication links, which are assumed to remain fixed within the interval  $[t_k, t_{k+1}]$ . A path from vertex  $v_0$  to vertex  $v_d$  is called a  $v_0 - v_d$  path and denoted as  $\mathcal{P}_k(v_0, v_d) = (v_0, v_1, \dots, v_d)$ , where  $v_0, v_1, \dots, v_d \in \mathcal{V}$  and  $\ell(\mathcal{P}_k(u, v))$  is the length of the path.

High-data rate FSO links are considered for the intra-plane ISLs since the relative distances and positions among these satellites are maintained, which minimizes pointing errors [5]. As a consequence, the intra-plane ISLs are fixed throughout the operation of the network and also possess a fixed data rate  $R_{\text{ISL}}$  and a fixed transmission power  $P_{\text{ISL}}$ .

Point-to-point satellite-to-ground links are established dynamically between the GS and the closest available satellite. Therefore, we define the edge set at time  $k$  as

$$\mathcal{E}_k = \left\{ (u, v) \cup (v_d, g) : u, v \in \mathcal{N}, v_d = \arg \min_{v \in \mathcal{N}} d_{t_k}(v, g) \right\}, \quad (6)$$

where  $d_{t_k}(v, g)$  is the Euclidean distance between satellite  $v$  and  $g$  at time  $t_k$ . The latter can be accurately calculated based on the ephemeris of the satellites for any  $t_k \in \mathbb{R}$  and, hence, our model operates with snapshots of the edge set taken at each  $t_k$ .

Differently from the intra-plane ISLs, the beams and data rate must be adapted continuously at the downlink due to the rapid movement of the satellites. Traditional RF technology is less prone to outages due to pointing errors and atmospheric conditions than FSO and, hence, it is used to achieve reliable communication to the GS.

We consider an interference-free additive-white Gaussian noise (AWGN) channel with free-space path loss and with noise power  $\sigma^2$ . Hence, the SNR for the satellite-to-ground link (i.e., downlink) at time  $t$  is given as

$$\gamma_t = G_{\text{tx}} G_{\text{rx}} P_{\text{tx}} \left( \frac{c}{4\pi d_t(v_d, g) f_c \sigma} \right)^2, \quad \text{where } v_d = \arg \min_v d_t(v, g) \quad (7)$$

where  $f_c$  is the carrier frequency,  $c = 2.998 \cdot 10^8$  m/s is the speed of light,  $G_d$  and  $G_g$  are the transmitter and receiver antenna gains, and  $P_{\text{tx}}$  is the transmission power of the space-to-ground satellite.

Once the SNR is known, a proper modulation and coding scheme can be selected to achieve reliable communication as described in the following. Let  $\mathcal{S}_{\text{DVB-S2}} = \{(R', \text{SNR}_{\min}(R'))\}$  be the

set of ordered pairs, containing a given spectral efficiency  $R'$  bits/s/Hz and the minimum SNR to achieve reliable communication with  $R'$ , namely  $\gamma_{\min}(R')$ , defined in the DVB-S2 system [15]. Then, the rate to transmit the packets for frame  $k$  is selected by adapting the modulation and coding scheme to achieve the maximum data rate for reliable communication within a period  $[t_k, t_k + \Delta t]$  as

$$R_k = B \max \{R' \in \mathcal{S}_{\text{DVB-S2}} : \min\{\gamma_t\} \geq \gamma_{\min}(R'), t \in [t_k, t_k + \Delta t]\}. \quad (8)$$

Similarly as for processing, we denote the queuing time at the communication module to transmit the data from  $u$  to  $v$  as  $Q_t^{\text{trans}}(u, v) \in \mathbb{R}^+$  seconds, where  $t$  is the time at which the data is received by  $u$ . Furthermore, we define the transmission time for a packet of size  $D_k$  as

$$L_k^{\text{trans}}(D_k, u, v) = \frac{D_k}{R_k(u, v)}, \quad (9)$$

where  $R_k(u, v) = R_{\text{ISL}}$  for all the ISLs and  $R_k(v_d, g) = R_k$  for the downlink.

#### D. Energy consumption

There are two contributors to the energy consumption at the satellite: the processing and compression of the images, and the communications.

We consider a model to calculate the energy consumption of the satellites due to the processing of the task that captures the most relevant CPU parameters [16]–[18]. In this model, the energy consumption per clock cycle is proportional to the square of the clock frequency of the CPU  $f_k$  times a constant  $\nu$ , which is the effective capacitance coefficient of the specific processor [17], [18]. Specifically,

$$E_{\text{cycle}}^{\text{proc}}(f_k^{(n)}) = \nu \cdot (f_k^{(n)})^2 = \frac{P_{\text{proc}}(f_{\text{CPU}})}{f_{\text{CPU}}^3} \cdot (f_k^{(n)})^2, \quad (10)$$

where  $P_{\text{proc}}(f_{\text{CPU}})$  is the power consumption during processing at the maximum CPU frequency. Building on this, and assuming that the supplied power is linear with the number of processor cores  $N_{\text{CPU}}$ , the energy consumption to process an image of size  $D_k$  bits is modeled as

$$E_k^{\text{proc}}(\rho_k, f_k^{(n)}; D_k, \epsilon) = D_k C(\rho_k, \epsilon) E_{\text{cycle}}^{\text{proc}}(f_k^{(n)}). \quad (11)$$

Regarding the energy consumption during communication, we consider two different models: one for the downlink (i.e., radio frequency link from the destination satellite to the GS) and another one for the FSO ISLs. For the downlink, we consider that the link only consumes energy during transmission and, hence, the energy consumption for the download of a segment

from frame  $k$  is simply  $P_{\text{tx}}D_k/R_k$ . On the other hand, we consider FSO links that may consume a non-negligible amount of energy during normal operation, that is, just to maintain the links. Specifically, let  $\eta \in [0, 1]$  be the fraction of energy consumption above normal operation during transmission with an FSO ISL. That is, we consider that the transmission power is  $P_{\text{ISL}}$  and  $\eta$  of that power is only consumed during transmission [19]. The remaining  $(1 - \eta)P_{\text{ISL}}$  is consumed during normal operation to maintain the FSO ISL. Therefore, we define

$$E_{\text{ISL}}^{\text{trans}}(D_k) = \frac{\eta P_{\text{ISL}} D_k}{R_{\text{ISL}}} \quad (12)$$

as the energy above normal operation that is required to transmit a packet of size  $D_k$  bits through an FSO ISL.

### III. PROBLEM FORMULATION

A task might consist of one or multiple frames, namely  $K$ , that are captured continuously by a source satellite  $v_0$ . Each of the  $k$  frames contains  $W_k \in \{0, 1, \dots\}$  images. The GS schedules the segmentation, processing, and transmission of the segments in a task jointly using its knowledge about the communication and processing capabilities of the satellites, along with the value of  $W_k$  for all  $k \in \mathcal{K}$ . For this, the GS builds an allocation matrix  $\mathbf{X} \in \mathbb{N}^{K \times N+1}$ , whose  $(k, n)$ -th element is  $x_k^{(n)}$ , indicating the amount of data from frame  $k$  that satellite  $n$  must process. Moreover, we denote the  $k$ -th row of  $\mathbf{X}$  as

$$\mathbf{x}_k = \left[ x_k^{(1)}, x_k^{(2)}, \dots, x_k^{(N)}, x_k^{(g)} \right], \quad (13)$$

which is the allocation vector for frame  $k$ . Naturally,

$$\mathbf{x}_k \mathbf{1} = \sum_{n=1}^N x_k^{(n)} + x_k^{(g)} = D_k \quad (14)$$

and the number of segments for frame  $k$ ,  $S_k$ , is the number of non-zero elements in vector  $\mathbf{x}_k$ .

The segment allocation is accompanied by matrix  $\mathbf{F} \in \mathbb{R}_+^{K \times N}$ , whose  $(k, n)$ -th element is  $f_k^{(n)}$  and defines the CPU frequency that must be selected by the satellite  $n$  for processing the segment from frame  $k$ . Finally, the GS must define the compression factor for each frame, defined by the vector  $\boldsymbol{\rho} = [\rho_1, \rho_2, \dots, \rho_K]$ .

We follow a resource slicing approach to ensure the stability of the processing and communication queues in the orbital plane. In such approach, the task is allocated an amount of processing and communication resources that is proportional to its duration  $KT_{\text{GTF}}$ . Therefore,

the processing and communication parameters for the task values must be selected to ensure that the average processing and transmission time of each segment, at each satellite and each link does not exceed the GTFP. Building on this, we formulate the following constraints.

*Processing constraint:* To ensure the stability of the processing queues at the satellite CPUs, the average time to process all the segments allocated to a given satellite  $n \in \mathcal{N}$ , of size  $\sum_{k=0}^K x_k^{(n)}$ , must be shorter than the duration of the task. Therefore, a proper CPU frequency must be selected for the processing of each segment at each satellite, denoted as  $f_k^{(n)}$ . From (5) we derive the processing constraint:

$$\sum_{k=1}^K \frac{x_k^{(n)} C(\rho_k, \epsilon)}{N_{\text{CPU}} f_k^{(n)}} \leq K T_{\text{GTF}}, \quad \forall n \in \mathcal{N}. \quad (15)$$

*Downlink and ISL rate constraints:* The average data rate for the satellite-to-ground link and the ISLs must be sufficiently high to transmit the generated data within the considered period of time of  $K T_{\text{GTF}}$  s. Hence, we formulate the downlink constraint as follows.

$$\sum_{k=1}^K \left( x_k^{(g)} + \frac{1}{\rho_k} \sum_{n=1}^N x_k^{(n)} \right) \leq T_{\text{GTF}}(h_{\text{px}}, d_{\text{gsd}}, h) \sum_{k=1}^K R_k \quad (16)$$

For the ISLs, the total amount of traffic depends on the scatter algorithm and the location of the processing satellites  $n \in \mathcal{N}_k$  w.r.t. the source satellite  $v_0$  and  $g$  for all the  $K$  frames. Specifically, to calculate the amount of traffic assigned to each ISL  $(u, v) \in \mathcal{E}_k$ , let  $\mathcal{P}_k(u, v)$  be the shortest path between  $u$  and  $v$  at time slot  $k$ . Next, we define the indicator variable  $y_k^{(e)}(u, v)$ , which takes the value of 1 if the edge  $e \in \mathcal{E}_k$  is in the path  $\mathcal{P}_k(u, v)$  and 0 otherwise. That is,

$$y_k^{(e)}(u, v) \triangleq \begin{cases} 1, & \text{if } e \in \mathcal{P}_k(u, v) \\ 0 & \text{otherwise.} \end{cases} \quad (17)$$

Based on the latter, we define the constraint for the data rate at the ISLs as

$$\sum_{k=1}^K x_k^{(g)} y_k^{(e)}(v_0, g) + \sum_{n=1}^N x_k^{(n)} \left( y_k^{(e)}(v_0, n) + \frac{y_k^{(e)}(n, g)}{\rho_k} \right) \leq K T_{\text{GTF}} R_{\text{ISL}}, \quad \forall e \in \mathcal{E}_k. \quad (18)$$

Nevertheless, in most practical scatter algorithms, the ISLs that communicate the source satellite  $v_0$  with its neighbors will be subject to the heaviest traffic. Therefore, the latter constraint can be simplified by limiting it to the ISLs  $\mathcal{E}_0 = \{(v_0, n) \in \mathcal{E} : n \in \mathcal{N}_k^{(n)}\}$

Further, recall that  $\ell(\mathcal{P}_k(u, v))$  is defined as the length of the  $u - v$  path. Then, we define the energy devoted for the *scatter* phase as

$$E_k^{\text{scatter}}(v_0, \mathbf{x}_k; \eta) = \frac{P_{\text{tx}} x_k^{(g)}}{R_k} + \frac{\eta P_{\text{ISL}}}{R_{\text{ISL}}} \left( \sum_{n=1}^N \ell(\mathcal{P}_k(v_0, n)) x_k^{(n)} + (\ell(\mathcal{P}_k(v_0, g)) - 1) x_k^{(g)} \right), \quad (19)$$

where the first addend corresponds to energy needed to reach the GS and the second one for the distribution among satellites. The parenthesis accounts for the amount of data that reaches each node, weighted by the number of steps (i.e., links). Likewise, the consumed energy for the *gather* phase is defined as

$$E_k^{\text{gather}}(\rho_k, \mathbf{x}_k; \eta) = \frac{1}{\rho_k} \sum_{n=1}^N x_k^{(n)} \left( \frac{P_{\text{tx}}}{R_k} + \frac{\eta P_{\text{ISL}}}{R_{\text{ISL}}} (\ell(\mathcal{P}_k(n, g)) - 1) \right), \quad (20)$$

where each compressed segment, i.e.,  $x_k^{(n)}/\rho_k$ , is weighted by the energy per bit it takes to reach the GS from each satellite  $n$  through ISL and RF links. The overall energy consumption, due to distribution and processing of the data, is defined as the sum of the energy at the scatter, processing, and gather phases. Hence, we formulate the energy minimization problem as

$$\begin{aligned} \text{P}_1 : \underset{\mathbf{X}, \mathbf{F}, \rho}{\text{minimize}} \quad & \sum_{k=1}^K E_k^{\text{scatter}}(v_0, \mathbf{x}_k; \eta) + E_k^{\text{gather}}(\rho_k, \mathbf{x}_k; \eta) + \sum_{n=1}^N E_k^{\text{proc}}\left(x_k^{(n)}, \rho_k, f_k^{(n)}; \epsilon\right) \quad (21) \\ \text{subject to} \quad & (15), (16), (18) \end{aligned}$$

$$0 \leq x_k^{(n)} \leq D_k, \quad \forall n \in \mathcal{N}, k \in \mathcal{K} \quad (21a)$$

$$\mathbf{x}_k \mathbf{1} = D_k, \quad \forall k \in \mathcal{K} \quad (21b)$$

$$1 < \rho_k \leq \rho_{\max}, \quad \forall k \in \mathcal{K} \quad (21c)$$

$$0 < f_k^{(n)} \leq f_{\text{CPU}}, \quad \forall k \in \mathcal{K}, n \in \mathcal{N}. \quad (21d)$$

where the parameter  $\rho_{\max}$  is a pre-defined maximum acceptable compression ratio.

That is, for each frame  $k \in \mathcal{K}$ , the GS must determine the compression ratio  $\rho_k$ , the allocation vector  $\mathbf{x}_k$ , and the CPU frequency  $f_k^{(n)}$  to minimize energy while fulfilling the processing and communication constraints. Note that constraint (22) is defined to avoid the value of  $\rho_k = 1$ , as this represents no processing at the satellites and is an equivalent solution to setting  $x_k^{(g)} = 1$ .

Naturally, the routing algorithm, which determines the paths to be followed by the segments, has an impact on the links used during the scatter and gather phases by determining the variables  $\ell(\mathcal{P}_k(v_0, n))$ ,  $\ell(\mathcal{P}_k(n, g))$ , and  $y_k^{(e)}(v_0, n)$  and  $y_k^{(e)}(n, g)$ . Consequently, the routing algorithm has an impact on the ISL constraint and on the energy consumption. Nevertheless, investigating the optimal routing algorithm for each phase is out of the scope of the paper and, hence, we consider a typical hop-count shortest-path routing algorithm and treat these variables as parameters in (21).

For the case with for  $C(\rho_k, \epsilon) = e^{\rho_k \epsilon} - e^\epsilon$ , neither the energy consumption for processing  $E_k^{\text{proc}}(\rho_k, f_k^{(n)}; D_k, \epsilon)$ , defined in (11), nor for communication in the gather phase  $E_k^{\text{gather}}(\rho_k, \mathbf{x}_k; \eta)$ ,

defined in (20) are jointly convex in  $\mathbf{X}$  and  $\boldsymbol{\rho}$ . Consequently, the objective function (21) is not jointly convex in  $\mathbf{X}$ ,  $\boldsymbol{\rho}$ , and  $\mathbf{F}$ . Furthermore, the constraints (15), (16), (18) are not jointly convex in  $\mathbf{X}$  and  $\boldsymbol{\rho}$ . Thus,  $P_1$  is a non-convex optimization problem. Nevertheless, we can exploit the fact that the problem is convex when only considering one optimization variable at a time. In particular, a closed-form expression can be obtained for the CPU frequency of the satellites  $\mathbf{F}$ . Furthermore,  $E_k^{\text{scatter}}(v_0, \mathbf{x}_k; \eta)$  is linear in  $\mathbf{X}$ . Therefore, we follow a variable decomposition approach and decompose the general optimization problem (21) into three sub-problems, which are solved iteratively following the Block Coordinate Descent (BCD) algorithm to reach a near-optimal solution [20]. Specifically, we begin by obtaining the closed-form solution for the optimal CPU frequency  $\mathbf{F}^*$ . The optimal CPU frequency is then used to optimize  $\mathbf{X}$  and  $\boldsymbol{\rho}$  iteratively.

Conversely, for the case with the JPEG compression algorithm  $C(\rho_k, \epsilon) = \epsilon$ , the optimal solution for the compression ratio is  $\rho_k = \rho_{\max}$ , which is treated as a parameter and the optimization problem (21) simplifies to only optimizing  $\mathbf{X}$  and  $\mathbf{F}$  jointly.

#### A. Optimizing the CPU frequency

As starting point, we consider the problem of optimizing the CPU frequency  $\mathbf{F}$  for a given  $\boldsymbol{\rho}$  and  $\mathbf{X}$  in  $P_1$ . We formulate the optimization problem for this case as

$$\begin{aligned}
 P_F : \underset{\mathbf{F}}{\text{minimize}} \quad & \sum_{n=1}^N \sum_{k=1}^K E_k^{\text{proc}} \left( x_k^{(n)}, \rho_k, f_k^{(n)}; \epsilon \right) \\
 \text{subject to} \quad & \sum_{k=1}^K \frac{x_k^{(n)} C(\rho_k, \epsilon)}{K N_{\text{CPU}} f_k^{(n)}} \leq T_{\text{GTF}} \quad \forall n \in \mathcal{N} \\
 & 0 \leq f_k^{(n)} \leq f_{\text{CPU}}, \quad \forall k \in \mathcal{K}, n \in \mathcal{N}.
 \end{aligned} \tag{22}$$

**Theorem 1** (Optimal CPU frequency). *If the problem is feasible for the given  $\mathbf{X}$  and  $\boldsymbol{\rho}$ , the optimal CPU frequency is constant and equals the minimum required to satisfy the processing constraint (15). Therefore, the optimal CPU frequency for satellite  $n$  given  $\mathbf{X}$  and  $\boldsymbol{\rho}$  is given by*

$$f_k^{(n)*} = f^{(n)} = \frac{\sum_{k=1}^K x_k^{(n)} C(\rho_k, \epsilon)}{K N_{\text{CPU}} T_{\text{GTF}}} \quad \forall n \in \mathcal{N} : \sum_{k=1}^K x_k^{(n)} C(\rho_k, \epsilon) - T_{\text{GTF}} K N_{\text{CPU}} f_{\text{CPU}} \leq 0 \tag{23}$$

. The proof is based on the complementary slackness condition and is presented in the Appendix A.

In all the cases where the processing constraint cannot be fulfilled, the CPU frequency is set momentarily to  $f^{(n)} = f_{\text{CPU}}$  to proceed with the iterative optimization.



### B. Optimizing the task allocation

Next, we define problem  $P_{\mathbf{X}}$ : optimizing  $\mathbf{X}$  for a given  $\mathbf{F}^*$  and  $\boldsymbol{\rho}$ . Based on the previous result for  $\mathbf{F}^*$ , we transform the constraint (15) and define the problem as

$$\begin{aligned}
P_{\mathbf{X}} : \underset{\mathbf{X}}{\text{minimize}} \quad & \sum_{k=1}^K \left( E_k^{\text{scatter}}(v_0, \mathbf{x}_k; \eta) + E_k^{\text{gather}}(\rho_k, \mathbf{x}_k; \eta) \right) + \sum_{n=1}^N E_k^{\text{proc}} \left( x_k^{(n)}, \rho_k, f^{(n)}; \epsilon \right) \quad (24) \\
\text{subject to} \quad & \sum_{k=1}^K x_k^{(n)} C(\rho_k, \epsilon) - KT_{\text{GTF}} N_{\text{CPU}} f^{(n)} \leq 0, \quad \forall n \in \mathcal{N}, \quad (24a) \\
& (16), (18) \\
& 0 \leq x_k^{(n)} \leq D_k, \quad \forall n \in \mathcal{N}, k \in \mathcal{K} \\
& \mathbf{x}_k \mathbf{1} = D_k, \quad \forall k \in \mathcal{K}
\end{aligned}$$

The latter problem is linear in  $\mathbf{X}$  with affine constraints and, since  $\mathbf{F}^*$  can be calculated in closed-form, we solve the problem using an iterative convex optimization approach with the augmented Lagrangian of (24a), where the processing constraint is moved to the objective and used as penalty [21]. Specifically,

$$\begin{aligned}
P_{\mathcal{L}(\mathbf{X}, \mathbf{F}^*; \alpha)} : \underset{\mathbf{X}}{\text{minimize}} \quad & \sum_{k=1}^K \left( E_k^{\text{scatter}}(v_0, \mathbf{x}_k; \eta) + E_k^{\text{gather}}(\rho_k, \mathbf{x}_k; \eta) \right) + \sum_{n=1}^N \left[ E_k^{\text{proc}} \left( x_k^{(n)}, \rho_k, f^{(n)}; \epsilon \right) \right. \\
& + \lambda^{(n)} \left( \sum_{k=1}^K \frac{x_k^{(n)} C(\rho_k, \epsilon)}{KT_{\text{GTF}} N_{\text{CPU}}} - f^{(n)} + s^{(n)} \right) \\
& \left. + \frac{\alpha}{2} \left( \sum_{k=1}^K \frac{x_k^{(n)} C(\rho_k, \epsilon)}{KT_{\text{GTF}} N_{\text{CPU}}} - f^{(n)} + s^{(n)} \right)^2 \right] \quad (25) \\
\text{subject to} \quad & (16), (18) \\
& 0 \leq x_k^{(n)} \leq D_k, \quad \forall n \in \mathcal{N}, k \in \mathcal{K} \\
& \mathbf{x}_k \mathbf{1} = D_k, \quad \forall k \in \mathcal{K}.
\end{aligned}$$

We solve problem (25) following the Penalty Dual Decomposition (PDD) method [22] by first solving for  $\mathbf{X}$  for a given  $\mathbf{F}$ . Then, the values of  $\mathbf{F}^*$  are updated after each iteration with the update rule in (23). Finally, as  $\mathbf{F}^*$  has been already updated, the slack variables  $s^{(n)}$  become 0. Then, following the PDD method, the Lagrange multipliers  $\lambda^{(n)}$  and the penalty terms  $\alpha^{(n)}$

are updated according to a pre-defined threshold  $\tau_{\text{proc}}$  and increase factor  $\beta \in (0, 1)$ . Namely, if the processing constraint is below a pre-defined threshold  $\tau_{\text{proc}}$ , the update rule for  $\lambda^{(n)}$  with inequality constraints becomes

$$\lambda^{(n)} = \max \left( 0, \lambda^{(n)} + \alpha^{(n)} \left( \sum_{k=1}^K x_k^{(n)} C(\rho_k, \epsilon) - T_{\text{GTF}} K N_{\text{CPU}} f^{(n)} \right) \right). \quad (26)$$

Otherwise, if the processing constraint is above  $\tau_{\text{proc}}$ , the penalty parameter is increased as  $\alpha^{(n)} \leftarrow \alpha^{(n)} / \beta$ .

### C. Optimizing the compression ratio

Finally, we proceed to optimize the compression factor  $\rho$  for a given  $\mathbf{X}$  and  $\mathbf{F}^*$  for the case where  $C(\rho_k, \epsilon)$  increases with  $\rho_k$ .

First, we formulate the optimization problem for  $\rho$  from (21) by removing the constant term  $E_k^{\text{scatter}}(v_0, \mathbf{x}_k; \eta)$  and the constraints on  $\mathbf{X}$ , which give

$$\mathbf{P}_\rho : \underset{\rho}{\text{minimize}} \quad \sum_{k=1}^K E_k^{\text{gather}}(\rho_k, \mathbf{x}_k; \eta) + \sum_{n=1}^N E_k^{\text{proc}}(x_k^{(n)}, \rho_k, f^{(n)}; \epsilon) \quad (27)$$

$$\text{subject to} \quad \sum_{k=1}^K x_k^{(n)} C(\rho_k, \epsilon) - K T_{\text{GTF}} N_{\text{CPU}} f^{(n)} \leq 0, \quad \forall n \in \mathcal{N}, \quad (27a)$$

(16), (18)

$$1 < \rho_k \leq \rho_{\text{max}} \quad \text{for all } k \in \mathcal{K}$$

Let  $\mathbf{s}$  be the vector of slack variables, which includes those for the downlink constraint  $s^{(g)}$ , for the ISL constraints  $s^{(e)}$  and for the values of  $\rho_k$ , namely  $s_k^{(\rho)}$ . Furthermore, we define the Lagrange multiplier and penalty terms for these constraints as  $\lambda^{(g)}$  and  $\alpha^{(g)}$ ,  $\lambda^{(e)}$  and  $\alpha^{(e)}$ , and  $\lambda_k^{(\rho)}$  and  $\alpha_k^{(\rho)}$ , respectively. Building on these, the augmented Lagrangian for the latter problem

is

$$\begin{aligned}
\mathcal{L}(\boldsymbol{\rho}, \boldsymbol{\lambda}, \mathbf{s}; \mathbf{X}, \boldsymbol{\alpha}) = & \\
& \sum_{k=1}^K E_k^{\text{gather}}(\rho_k, \mathbf{x}_k; \eta) + \sum_{n=1}^N \left[ E_k^{\text{proc}}\left(x_k^{(n)}, \rho_k, f^{(n)}; \epsilon\right) \right. \\
& \left. + \lambda^{(n)} \left( \sum_{k=1}^K \frac{x_k^{(n)} C(\rho_k, \epsilon)}{K N_{\text{CPU}} T_{\text{GTF}}} - f^{(n)} + s^{(n)} \right) + \frac{\alpha^{(n)}}{2} \left( \sum_{k=1}^K \frac{x_k^{(n)} C(\rho_k, \epsilon)}{K N_{\text{CPU}} T_{\text{GTF}}} - f^{(n)} + s^{(n)} \right)^2 \right] \\
& + \lambda^{(g)} \left[ s^{(g)} + \sum_{k=1}^K \frac{x_k^{(g)} + \sum_{n=1}^N \frac{x_k^{(n)}}{\rho_k}}{T_{\text{GTF}}} - R_k \right] + \frac{\alpha^{(g)}}{2} \left[ s^{(g)} + \sum_{k=1}^K \frac{x_k^{(g)} + \sum_{n=1}^N \frac{x_k^{(n)}}{\rho_k}}{T_{\text{GTF}}} - R_k \right]^2 \\
& + \sum_{e \in \mathcal{E}_s} \lambda^{(e)} \left[ s^{(e)} + \sum_{k=1}^K \frac{x_k^{(g)} y_k^{(e)}(v_0, g)}{K T_{\text{GTF}} R_{\text{ISL}}} + \sum_{n=1}^N \frac{x_k^{(n)} \left( y_k^{(e)}(v_0, n) + \frac{y_k^{(e)}(n, g)}{\rho_k} \right)}{K T_{\text{GTF}} R_{\text{ISL}}} \right] \\
& + \sum_{e \in \mathcal{E}_s} \frac{\alpha^{(e)}}{2} \left[ s^{(e)} + \sum_{k=1}^K \frac{x_k^{(g)} y_k^{(e)}(v_0, g)}{K T_{\text{GTF}} R_{\text{ISL}}} + \sum_{n=1}^N \frac{x_k^{(n)} \left( y_k^{(e)}(v_0, n) + \frac{y_k^{(e)}(n, g)}{\rho_k} \right)}{K T_{\text{GTF}} R_{\text{ISL}}} \right]^2 \\
& + \sum_{k=1}^K \lambda_k^{(\rho)} \left( \rho_k - \rho_{\max} + s_k^{(\rho)} \right) + \sum_{k=1}^K \frac{\alpha_k^{(\rho)}}{2} \left( \rho_k - \rho_{\max} + s_k^{(\rho)} \right)^2 \tag{28}
\end{aligned}$$

Note that the neither the slack variables for the downlink constraint nor for the ISL constraints depend on  $k$  as the limiting factors are the average rates throughout the execution of the task.

Then, the problem becomes

$$\begin{aligned}
& \underset{\boldsymbol{\rho} \geq 1, \mathbf{s} \geq 0}{\text{minimize}} \quad \underset{\boldsymbol{\lambda} \geq 0, \lambda^{(n)}, \lambda_k}{\text{maximize}} \quad \mathcal{L}(\mathbf{X}, \boldsymbol{\rho}, \boldsymbol{\lambda}, \mathbf{s}; \boldsymbol{\alpha}), \tag{29}
\end{aligned}$$

which we solve using the method of projected gradient descent by applying the following update rules for  $\boldsymbol{\lambda}$  after updating  $\mathbf{F}$  according to (23) and  $\lambda^{(n)}$  according to (26).

$$\lambda^{(g)} = \max \left( 0, \lambda^{(g)} + \alpha^{(g)} \left[ s^{(g)} + \sum_{k=1}^K \frac{1}{T_{\text{GTF}}} \left( x_k^{(g)} + \sum_{n=1}^N \frac{x_k^{(n)}}{\rho_k} \right) - R_k \right] \right) \tag{30}$$

$$\lambda^{(e)} = \max \left( 0, \lambda^{(e)} + \alpha^{(e)} \left[ s^{(e)} + \sum_{k=1}^K \frac{x_k^{(g)} y_k^{(e)}(v_0, g)}{K T_{\text{GTF}} R_{\text{ISL}}} + \sum_{n=1}^N \frac{x_k^{(n)} \left( y_k^{(e)}(v_0, n) + \frac{y_k^{(e)}(n, g)}{\rho_k} \right)}{K T_{\text{GTF}} R_{\text{ISL}}} \right] \right) \tag{31}$$

$$\lambda_k^{(\rho)} = \max \left( 0, \lambda_k^{(\rho)} + \alpha_k^{(\rho)} \left( \rho_k - \rho_{\max} - s_k^{(\rho)} \right) \right) \tag{32}$$

---

**Algorithm 1** BCD algorithm for iterative non-convex optimization.

---

**Input:**  $K, R_{\text{ISL}}, W_k, \mathcal{G}_k, R_k$  for all  $k \in \mathcal{K}$  and tolerance  $\delta$

- 1: Calculate  $\mathcal{P}_k(v_0, n), y_k^{(e)}(v_0, n), \mathcal{P}_k(n, g)$  and  $y_k^{(e)}(n, g)$  for all  $n \in \mathcal{N}$  and  $k \in \mathcal{K}$
  - 2: Initialize  $x_k^{(v_0)} \leftarrow D_k, x_k^{(n)} = x_k^{(g)} \leftarrow 0$  for all  $n \neq s$ , and  $\rho_k \leftarrow \rho_k^{\text{init}}$  for all  $k \in \mathcal{K}$ , and  $f^{(n)} \leftarrow f_{\text{CPU}}$  for all  $n$
  - 3:  $\mathbf{X}' \leftarrow \mathbf{0}$  and  $\boldsymbol{\rho}' \leftarrow \mathbf{0}$
  - 4: **while**  $\|\mathbf{X} - \mathbf{X}'\|_2 + \|\boldsymbol{\rho} - \boldsymbol{\rho}'\|_2 > \delta$  **do**
  - 5:   **while**  $\|\mathbf{X} - \mathbf{X}'\|_2 > \delta$  **do**
  - 6:      $\mathbf{X}' \leftarrow \mathbf{X}$
  - 7:     Optimize  $\mathbf{X}$  given  $\mathbf{F}^*$  and  $\boldsymbol{\rho}$  with PDD (25)
  - 8:     Update  $\mathbf{F}^*$  given  $\mathbf{X}$  and  $\boldsymbol{\rho}$  as in (23)
  - 9:   **end while**
  - 10: **while**  $\|\boldsymbol{\rho} - \boldsymbol{\rho}'\|_2 > \delta$  **do**
  - 11:     $\boldsymbol{\rho}' \leftarrow \boldsymbol{\rho}$
  - 12:    Optimize  $\boldsymbol{\rho}$  given  $\mathbf{F}^*$  and  $\mathbf{X}$  with projected gradient descent as in (28)
  - 13:    Update  $\mathbf{F}^*$  given  $\mathbf{X}$  and  $\boldsymbol{\rho}$  as in (23)
  - 14: **end while**
  - 15: **end while**
  - 16: **return**  $\mathbf{X}^* \leftarrow \mathbf{X}, \boldsymbol{\rho}^* \leftarrow \boldsymbol{\rho}$ , and  $\mathbf{F}^*$
- 

Algorithm 1 illustrates the iterative procedure for global optimization for the case where  $C(\rho_k, \epsilon) = e^{\rho_k \epsilon} - e^\epsilon$ . Note that a feasible value for each  $\rho_k$  must be selected during initialization. For instance, we initialize each  $\rho_k$  with the value

$$\rho_k^{\text{init}} = \min \left\{ \max \left( 1, \frac{D_k}{T_{\text{GTF}} R_k} \right), \rho_{\text{max}} \right\}. \quad (33)$$

#### IV. RESULTS

We consider an orbital plane with  $N = 20$  satellites capturing images in an HD format with  $1920 \times 1080$  pixels under the following two scenarios.

- *Per-frame optimization*: Optimizing one frame independently is optimal if the task is relatively long (i.e.,  $K \rightarrow \infty$ ) and the frame size is constant  $W_k = W_{k'}$  for all  $k, k' \in \mathcal{K}$  and, naturally, if  $K = 1$ .

- *Multi-frame optimization:* In all cases, optimizing across the  $K$  frames of the task is the optimal approach. We illustrate the gains of this approach with respect to per-frame optimization in a synthetic scenario that leads to the upper bound in energy savings and in a realistic scenario that leads to the lower bound in energy savings.

Without loss of generality, the source satellite is denoted as  $v_0$ . The destination satellite  $v_d$  is assumed to be located at the edge of coverage at the first frame of the task and moves towards the center of coverage. The default parameters for the performance analysis are listed in Table II. With these parameters, the downlink data rate at the edge of coverage area is 2.16 Gbps. The GSD is set to  $d_{\text{gsd}} = 0.5$  m, which results in a GTFP of 78 ms.

The results were obtained through a simulator coded in Python, which replicates the orbital dynamics of the satellites and was used to calculate the data rates at each time slot. The optimization problems were solved using the CVXPY package [23] using MOSEK ApS as solver.

#### A. Per-frame optimization

Fig. 3 shows the energy consumption per image for the feasible values of  $W_k$  for direct download, local processing, and the global optimal solution. Two topologies are considered: 1) in Fig. 3b the destination satellite is the same as the source satellite  $v_d = v_0$  and 2) in Fig. 3d the destination satellite is  $v_d = v_5$ , namely, it's five hops away from the source satellite. Besides, two values are considered for parameter  $\eta = \{0.1, 1\}$ , which defines the fraction of energy consumption above normal operation for transmission with the FSO ISLs.

As it can be seen in Fig. 3, the energy consumption with direct download is much higher when compared to local processing and to the global optimal. Furthermore, direct download is only feasible with  $W_k \leq 3$  images. In contrast, local processing achieves a similar energy consumption as the global optimal for most of the cases within it's feasible region, which is  $6\times$  larger than with direct download, supporting up to  $W_k = 18$  images. Finally, the global optimal solution leads to the minimum energy consumption in all cases and also increases the feasible region by a factor of 12 when compared to direct download and by a factor of 2 when compared to local processing. Specifically, with the global optimal, the highest feasible value is  $W_k \leq 37$  for  $v_d = v_0$  (see Fig. 3a and Fig. 3b) and is  $W_k \leq 36$  for  $v_d = v_5$  (see Fig. 3c and Fig. 3d). The slight difference between these two topologies is because the data rate at the ISL ( $v_0, v_1$ ) is insufficient to further distribute the task for  $W_k = 37$  and  $v_d = v_5$ .

TABLE II  
PARAMETERS FOR PARALLEL PROCESSING

Parameter	Symbol	Setting
Altitude of deployment (km)	$h$	600
Number of satellites	$N$	20
Processor frequency (GHz)	$f_{\text{CPU}}$	1.8
Number of processor cores	$N_{\text{cores}}$	4
Power consumption for processing (W)	$P_{\text{proc}}(f_{\text{CPU}})$	10
Data rate of the ISLs (Gbps)	$R_{\text{ISL}}$	10
Transmission power of the ISLs (W)	$P_{\text{ISL}}$	60
Downlink transmission power (W)	$P_{\text{tx}}$	10
Downlink carrier frequency (GHz)	$f_c$	20
Downlink bandwidth (MHz)	$B$	500
Downlink antenna gain (dBi)	$G_d$	32.13
Antenna gain of the GS (dBi)	$G_g$	34.20
Width of the $k$ -th frame (images)	$W_k$	$\{0, 1, 2, \dots\}$
Size of HD image (MB)	$D_{\text{img}}$	5.93
Ground sample distance (GSD) (m/pixel)	$d_{\text{gsd}}$	0.5
Maximum compression factor	$\rho_{\text{max}}$	20
Complexity of the image processing algorithm	$\epsilon$	0.1
Fraction of energy consumption above normal operation during transmission with the ISL	$\eta$	$\{0.1, 1\}$

In addition, the energy consumption per image is considerably lower in Fig. 3b than in Fig. 3d due to the increased distance from the destination and, hence, the increase in the energy required for communication at the gather phase. In addition, the energy consumption with  $\eta = 0.1$  (see Fig. 3a and Fig. 3c) is considerably lower than that with  $\eta = 1$  (see Fig. 3b and Fig. 3d).

As a complement to the energy consumption per frame, Fig. 4 shows the selected value of  $\rho$  as a function of  $W_k$ . Clearly, the same value of  $\rho_k = \rho_k^*$  is selected by both the global optimal and the local processing approaches. Specifically,  $\rho_k^*$  decreases as  $W_k$  increases up to  $W_k = 9$  for  $v_d = v_0$  and up to  $W_k = 14$  for  $v_d = v_5$ . As  $W_k$  increases beyond these values, the optimal compression ratio is  $\rho_k^* = D_k/R_k$ , which is the lowest value that ensures feasibility and, hence, it can be easily selected with minimal computational resources for optimization.

We conclude the analyses of the per-frame optimization scenario by illustrating the values of

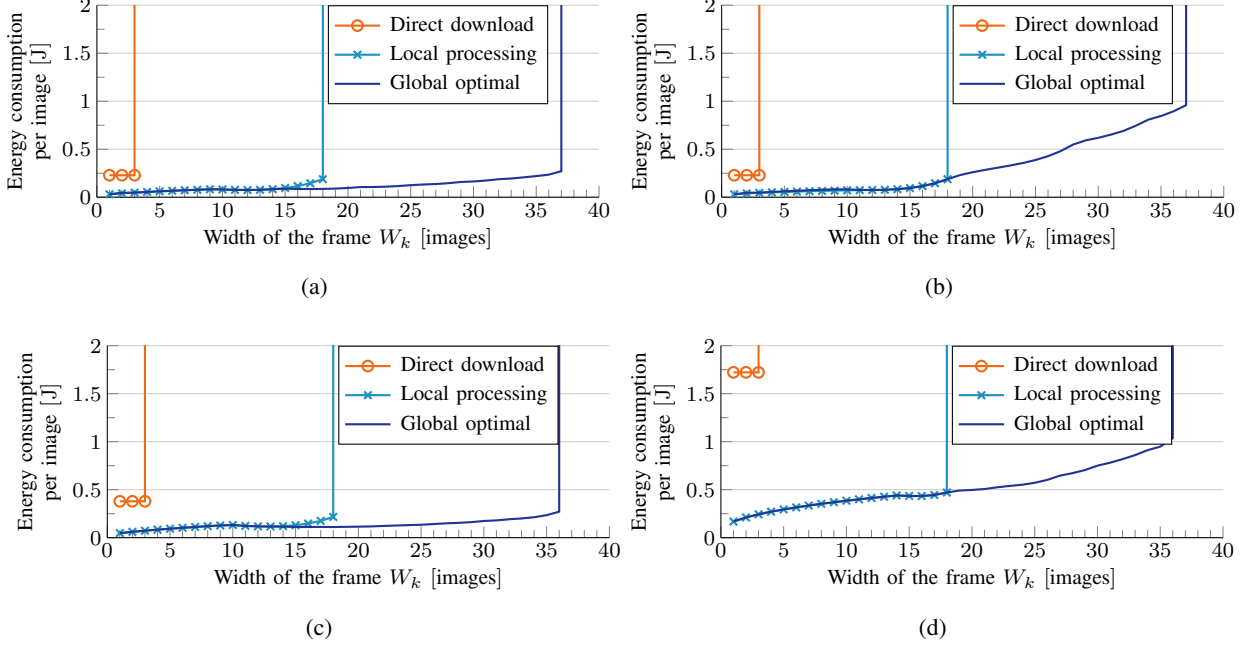


Fig. 3. Energy consumption per image for  $d_{gsd} = 0.5$  m with per-frame optimization for the cases where the destination satellite is  $v_d = v_0$  (a) with  $\eta = 0.1$  and (b) with  $\eta = 1$  and where the destination satellite is  $v_d = v_5$  (c) with  $\eta = 0.1$  and (d) with  $\eta = 1$  considering the three approaches: direct download, local processing, and global optimal. The energy consumption is set to  $\infty$  outside the feasible region.

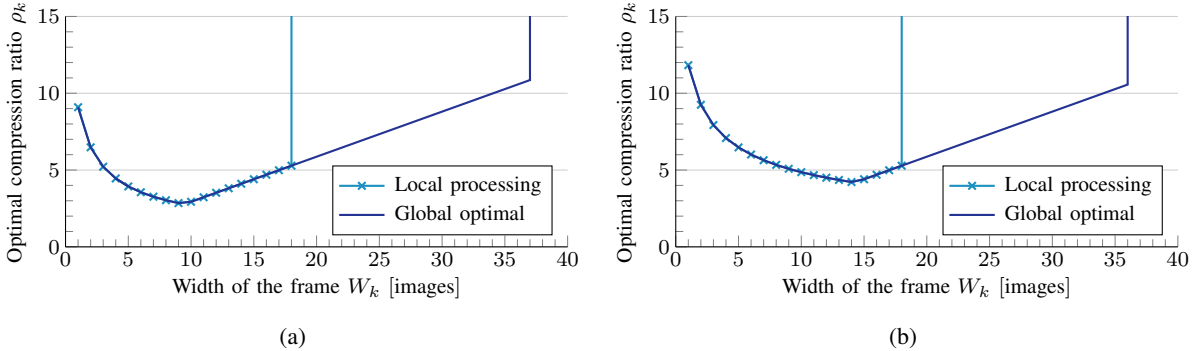


Fig. 4. Optimal compression ratio for  $K = 1$  considering for local processing and global optimal for (a)  $v_d = v_0$  and (b)  $v_d = v_5$ .

$\mathbf{x}_k^*$  in Fig. 5 for  $v_d = v_0$  and  $v_d = v_5$  with  $\eta = \{0.1, 1\}$ . Clearly, Fig. 5 shows that the data to process at neighboring SMEC nodes increases as  $W_k$  increases. Specifically, as shown in Fig. 5b and Fig. 5a, when the source satellite has direct connection to the GS, the data is distributed symmetrically across neighbouring satellites in the SMEC cluster. Conversely, for the case with  $v_d = v_5$  shown in Fig. 5d and Fig. 5c, a larger amount of the data is distributed to satellites in the

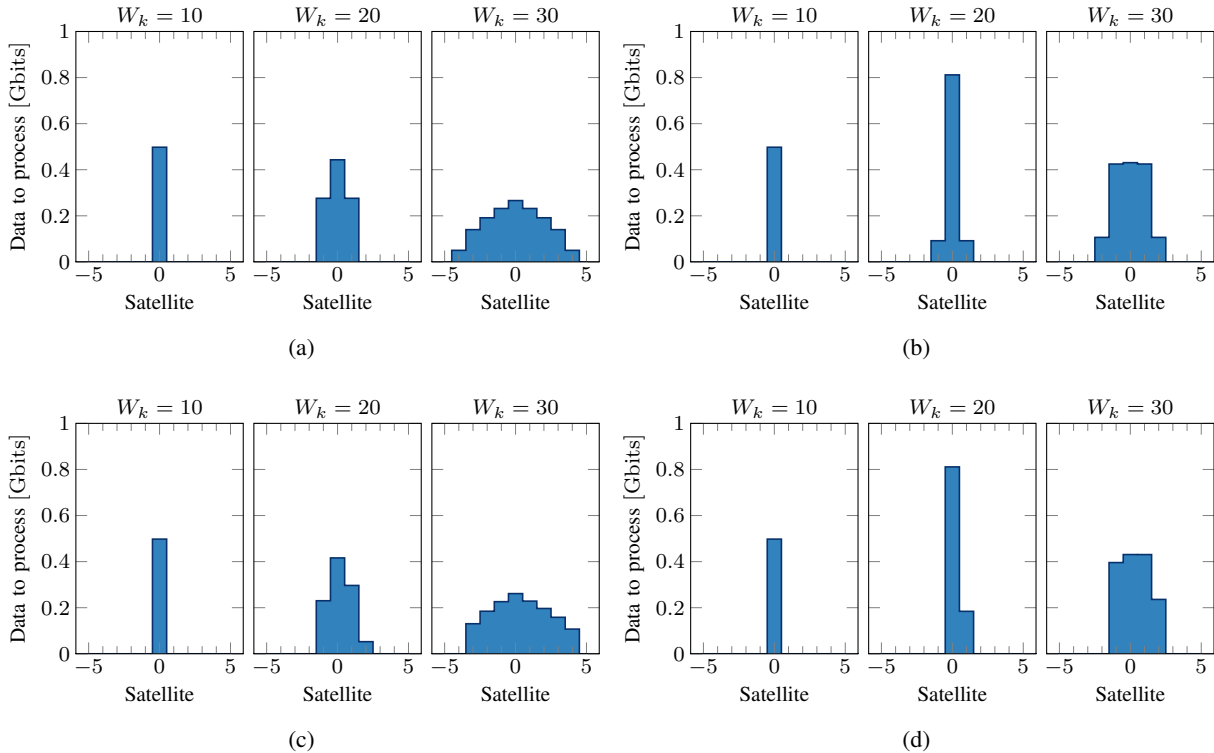


Fig. 5. Amount of data processed at the SMEC cluster for  $W_k = \{5, 10, 15, 20\}$  for  $v_d = v_0$  with (a)  $\eta = 0.1$  and (b)  $\eta = 1$  and for  $v_d = v_5$  with (c)  $\eta = 0.1$  and (d)  $\eta = 1$ .

SMEC cluster that are in the shortest path towards the destination. Furthermore, more satellites are used for processing for the case with  $\eta = 0.1$  (see Fig. 5a and Fig. 5c) when compared to the case with  $\eta = 1$  (see Fig. 5b and Fig. 5d). In all cases, the amount of data downloaded without processing is  $x_k^{(g)} = 0$ .

### B. Multi-frame optimization

Next, we compare the energy consumption that can be achieved by performing multi-frame optimization with respect to per-frame optimization.

First, we consider a scenario where the amount of tasks per GTFP is relatively low and the scheduler can dedicate an extended duration per task to reduce energy consumption. This is modeled by defining an initial frame of width  $W_0$  images followed by  $K - 1$  empty frames (i.e., with  $W_k = 0$  for  $k > 0$ ).

The energy consumption for  $W_0 = \{10, 20, 30\}$  with  $K = \{1, 2, 3, 4, 5\}$  is shown in Fig. 6 considering  $v_d = v_0$  in Fig. 6a and  $v_d = v_5$  in Fig. 6b. As it can be seen, the energy consumption



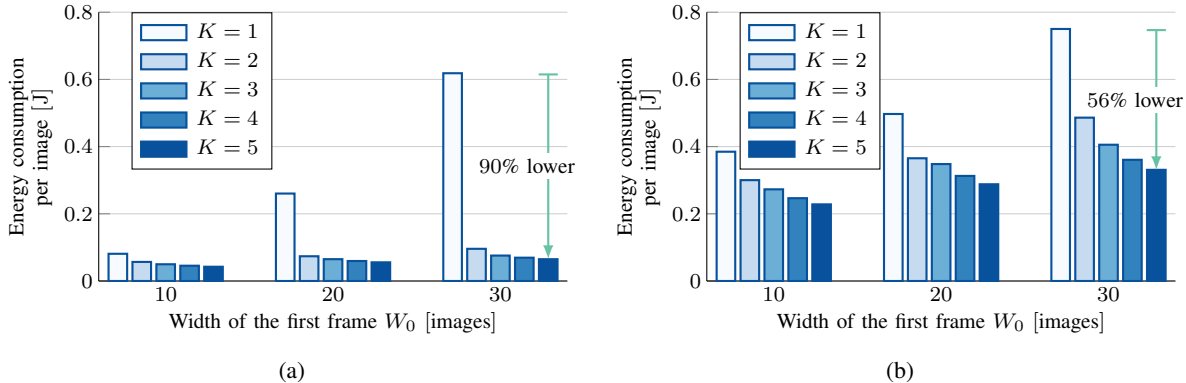


Fig. 6. Global optimal energy consumption for a task with  $K$  frames for  $\eta = 1$ , where the first frame contains  $W_0 \in \{5, 10, 15, 20\}$  images and the remaining  $K - 1$  frames are empty, i.e.,  $W_k = 0$  for  $k > 0$ . (a)  $v_d = v_0$  and (b)  $v_d = v_5$ .

increases drastically with the width of the frame  $W_0$  for the case with  $K = 1$ , which has zero empty frames. Nevertheless, the increase in energy consumption as  $W_k$  increases is lesser for all the cases with  $K > 1$  and the energy consumption per image is monotonously decreasing as  $K$  increases. Ultimately, the energy consumption with  $K = 5$ , which contains 4 empty frames, is 90% lower than with  $K = 1$  for the case with  $v_d = v_0$  and 56% lower than with  $K = 1$  for the case with  $v_d = v_5$ .

We conclude our analyses by evaluating the energy savings for the case of a realistic task of scanning the island of La Palma with  $v_d = v_5$ . Such task comprises  $K = 82$  frames with different widths  $W_k \in [1, 29]$  as shown in Fig. 7a. The pass of the satellite over La Palma takes 6.4 s, which is also the total duration of the task and occurs from top to bottom of the area shown in Fig. 7a and no empty frames are included in the task. Neither direct download nor local processing are feasible in this scenario due to the large number of images that must be captured.

Fig. 7b shows the energy consumption per image with per-frame optimization and with global optimization for  $\eta = \{0.1, 1\}$  for scanning the island of La Palma. Naturally, the energy consumption with  $\eta = 0.1$  is much lower than with  $\eta = 1$  as the energy consumption for transmission at the ISLs is  $10\times$  greater for the latter case. Most importantly, Fig. 7b shows that the global optimization across all the  $K = 82$  frames results in saving 9% and 11% of the energy when compared to per-frame optimization for  $\eta = 0.1$  and  $\eta = 1$ , respectively. Therefore, even though these energy savings are lesser than for the case with  $K - 1$  empty frames, they still represent an important reduction in energy consumption given that they are calculated with

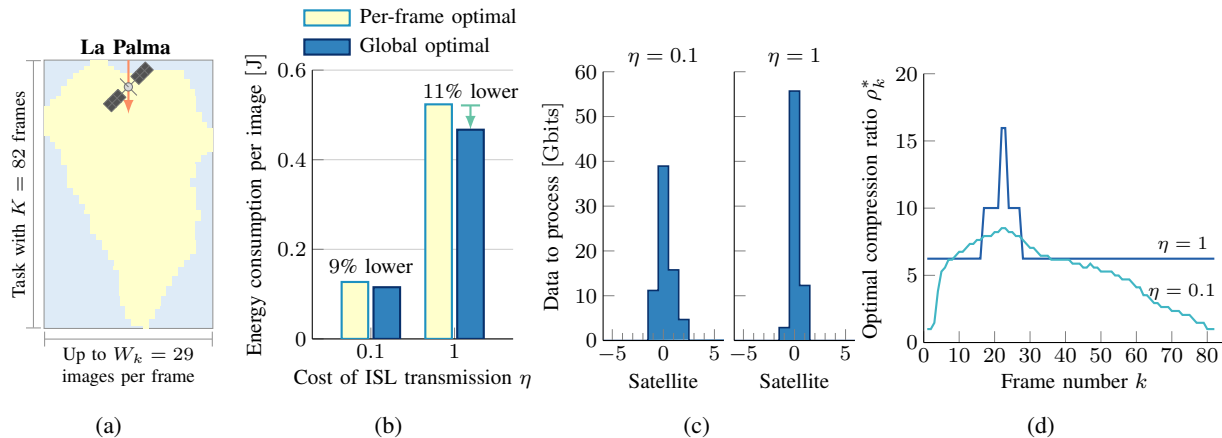


Fig. 7. (a) Task characteristics, (b) energy savings, (c) task allocation, and (d) optimal value of  $\rho_k$  for scanning La Palma island with a GSD of  $d_{\text{gsd}} = 0.5$  m.

respect to the optimal values when considering the frames independently, whose results are presented in Fig. 3c and Fig. 3d.

Finally, Figs. 7c and 7d show the optimal total amount of data allocated to each satellite  $\sum_{k=1}^K x_k^{(n)}$  (i.e., throughout the  $K = 82$  frames) and the optimal compression ratio  $\rho_k^*$ . Figs. 7c shows that the number of satellites in the SMEC cluster and the total amount of data allocated to each of them for processing changes with the value of  $\eta$ . Specifically, if  $\eta = 0.1$ , the data is more evenly distributed across 4 satellites than with  $\eta = 1$ , where the source satellite processes more than 78% of the total amount of data.

Finally, Fig. 7d shows that the optimal compression ratio for each frame  $\rho_k^*$  is not uniform across the task and, in general, increases with the number of images in the frame. Furthermore, the values of  $\rho_k^*$  are widely different for the two considered values of  $\eta$ , which illustrates the need for the careful selection of  $\rho_k^*$  based on the task allocation and the cost of transmission.

## V. CONCLUSIONS

Despite the distances between LEO satellites are much larger than those in terrestrial networks, distributed SMEC offers many benefits for very-high resolution Earth observation applications. In this paper, we considered a scenario where the physical characteristics of the system, dictated by the orbital parameters of the satellites and the area covered by their camera, determine the real-time requirements, which are necessary to maintain stability in the communication links and in the CPUs of the satellites. Moreover, we presented a general framework and an iterative

optimization method for distributed SMEC. Our results show that distributed SMEC allows to capture, process, and download up to  $6\times$  more images than with direct download and up to  $2\times$  more images than with local SMEC. Furthermore, up to 90% of the energy can be saved by carefully selecting the allocation of data, the compression ratio, and the processing frequency at the satellites. Finally, we considered a real-life task and observed that 1) it is only feasible to complete the task with distributed SMEC and 2) optimizing the task parameters jointly leads to additional energy savings when compared to optimizing each frame independently. These benefits set the basis for achieving very-high resolution Earth observation missions.

## APPENDIX

To obtain the closed-form expression for the optimal CPU frequency, observe that the energy for processing increases monotonically with  $f_k^{(n)}$ . Furthermore, the problem is feasible with a given  $\mathbf{X}$  and  $\boldsymbol{\rho}$  if and only if  $\exists F : 0 \leq f_k^{(n)} \leq f_{\text{CPU}}$  for all  $n$  and  $k$  that satisfies (15).

To find the closed-form expression for the optimal CPU frequency, we define the Lagrangian of  $P_F$ , defined in (22) as

$$\begin{aligned} \mathcal{L}(\mathbf{F}, \boldsymbol{\lambda}) = & \sum_{n=1}^N \left( \sum_{k=1}^K \nu C(\rho_k, \epsilon) x_k^{(n)} \left( f_k^{(n)} \right)^2 + \lambda^{(n)} \left( \sum_{k=1}^K \frac{x_k^{(n)} C(\rho_k, \epsilon)}{K N_{\text{CPU}} f_k^{(n)}} - T_{\text{GTF}} \right) \right. \\ & \left. + \sum_{k=1}^K \lambda_k^{(n)} \left( f_k^{(n)} - f_{\text{CPU}} \right) \right) \end{aligned} \quad (34)$$

From complementary slackness [24], we have that an optimal solution to the primal and dual problem satisfies the following two conditions.

$$\lambda^{(n)} \left( \sum_{k=1}^K \frac{x_k^{(n)} C(\rho_k, \epsilon)}{K N_{\text{CPU}} f_k^{(n)}} - T_{\text{GTF}} \right) = 0, \quad (35)$$

$$\sum_{n=1}^N \sum_{k=1}^K \lambda_k^{(n)*} \left( f_k^{(n)*} - f_{\text{CPU}} \right) = 0. \quad (36)$$

Thus, we express the first complementary slackness condition (35) as

$$\sum_{k=1}^K \frac{x_k^{(n)} C(\rho_k, \epsilon)}{f_k^{(n)}} < T_{\text{GTF}} K N_{\text{CPU}} \implies \lambda^{(n)} = 0, \quad (37)$$

otherwise

$$\lambda^{(n)} > 0 \implies \sum_{k=1}^K \frac{x_k^{(n)} C(\rho_k, \epsilon)}{f_k^{(n)}} = T_{\text{GTF}} K N_{\text{CPU}}. \quad (38)$$

For condition (36) we have that

$$f_k^{(n)*} < f_{\text{CPU}} \implies \lambda_k^{(n)*} = 0. \quad (39)$$

Otherwise,

$$\lambda_k^{(n)*} > 0 \implies f_k^{(n)*} = f_{\text{CPU}}. \quad (40)$$

Next, by taking the gradient of the Lagrangian  $\mathcal{L}(\mathbf{F}, \boldsymbol{\lambda})$  w.r.t.  $f_k^{(n)}$  we have

$$\nabla_{f_k^{(n)}} \mathcal{L}(\mathbf{F}, \boldsymbol{\lambda}) = 2\nu C(\rho_k, \epsilon) x_k^{(n)} f_k^{(n)} - \frac{\lambda_k^{(n)} x_k^{(n)} C(\rho_k, \epsilon)}{KN_{\text{CPU}} \left(f_k^{(n)}\right)^2} + \lambda_k^{(n)} = 0. \quad (41)$$

In the following, we consider the solution of problem  $P_F$  for the cases where  $C(\rho_k, \epsilon) x_k^{(n)} > 0$ .

**Case 1:** To fulfill condition (39), the optimal value of the multiplier obtained from (41) is

$$\lambda_k^{(n)*} = 2\nu KN_{\text{CPU}} \left(f_k^{(n)*}\right)^3, \quad \text{s.t. } f_k^{(n)*} < f_{\text{CPU}} \text{ and } \lambda_k^{(n)*} = 0 \text{ for all } k \in \mathcal{K}, \quad (42)$$

Therefore, we conclude that an equal solution  $f^{(n)} = f_k^{(n)*} < f_{\text{CPU}}$  is obtained for all  $k \in \mathcal{K}$ .

That is, for any given satellite  $n \in \mathcal{N}$ , the optimal CPU frequency is equal for all the frames in a task. Furthermore, this implies that, if  $\exists \lambda_k^{(n)} = 0$  for  $k \in \mathcal{K}$ , then  $\lambda_k^{(n)} = 0$  for all  $k \in \mathcal{K}$ .

Specifically, by substituting  $f_k^{(n)*}$  with  $f^{(n)}$  in (38), we obtain

$$f^{(n)} = \frac{1}{KN_{\text{CPU}} T_{\text{GTF}}} \sum_{k=1}^K x_k^{(n)} C(\rho_k, \epsilon) \quad (43)$$

Furthermore, note that from (38) and (42), the following condition must hold

$$f^{(n)} \in (0, f_{\text{CPU}}) \implies \lambda_k^{(n)*} > 0. \quad (44)$$

Nevertheless, the latter does not prevent the case where  $f^{(n)} = f_{\text{CPU}}$  and  $\lambda_k^{(n)*} = 0$  and, therefore (43) is the optimal solution for all cases where  $\lambda_k^{(n)} = 0$ .

**Case 2:** To fulfill condition (37), the optimal value of the multiplier obtained from (41) is

$$\lambda_k^{(n)*} = -2\nu C(\rho_k, \epsilon) x_k^{(n)} f_k^{(n)*} \quad (45)$$

Since all the terms on the right-hand side of (45) are either positive or zero and it is required that  $\lambda_k^{(n)*} \geq 0$ , then the only solutions to fulfill (45) lead to  $\lambda_k^{(n)*} = \lambda_k^{(n)*} = 0$  and are as follows.

If there is no data to process at satellite  $n$ , any CPU frequency can be selected, namely,

$$C(\rho_k, \epsilon) x_k^{(n)} = 0 \implies f_k^{(n)*} \in [0, f_{\text{CPU}}], \quad (46)$$

which means that the value of  $f_k^{(n)}$  is irrelevant.

The other option is when the satellite  $n$  has data to process

$$C(\rho_k, \epsilon)x_k^{(n)} > 0 \implies f_k^{(n)*} = 0, \quad (47)$$

but the latter option makes the processing time to be infinite, so it should be excluded from the set of possible solutions. Consequently, conditions (37) and (39) can only be fulfilled jointly if the satellite has no data to process. In other words, there is no optimal solution where  $f_k^{(n)*} < f_{\text{CPU}}$  and that leads to a processing time lesser than  $T_{\text{GTF}}$ .

## REFERENCES

- [1] M. Herold, C. E. Woodcock, T. R. Loveland, J. Townshend, M. Brady, C. Steenmans, and C. C. Schmullius, "Land-cover observations as part of a Global Earth Observation System of Systems (GEOSS): Progress, activities, and prospects," *IEEE Systems Journal*, vol. 2, no. 3, pp. 414–423, 2008.
- [2] M. Drusch, U. D. Bello, S. Carlier, O. Colin, V. Fernandez, F. Gascon, B. Hoersch, C. Isola, P. Laberinti, P. Martimort, A. Meygret, F. Spoto, O. Sy, F. Marchese, and P. Bargellini, "Sentinel-2: ESA's optical high-resolution mission for GMES operational services," *Remote Sensing of Environment*, vol. 120, pp. 25–36, 5 2012.
- [3] B. Denby and B. Lucia, "Orbital edge computing: Machine inference in space," *IEEE Computer Architecture Letters*, vol. 18, no. 1, pp. 59–62, Jan. 2019.
- [4] —, "Orbital edge computing: Nanosatellite constellations as a new class of computer system," in *Proc. International Conference on Architectural Support for Programming Languages and Operating Systems (ASPLOS)*, mar 2020, pp. 939–954.
- [5] H. Kaushal and G. Kaddoum, "Optical communication in space: Challenges and mitigation techniques," *IEEE Communications Surveys & Tutorials*, vol. 19, no. 1, pp. 57–96, 2017.
- [6] M. M. Gost, I. Leyva-Mayorga, A. Pérez-Neira, M. A. Vázquez, B. Soret, and M. Moretti, "Edge computing and communication for energy-efficient Earth surveillance with LEO satellites," in *Proc. IEEE Int. Conf. Commun. (ICC) Workshops*, 2022, pp. 556–561.
- [7] K. B. Alici, F. S. Oktem, O. Karci, A. S. Yilmaz, and O. Selimoglu, "Image chain simulation for earth observation satellites," *IEEE Journal of Selected Topics in Applied Earth Observations and Remote Sensing*, vol. 12, pp. 4014–4023, 10 2019.
- [8] J.-B. Wang, J. Zhang, C. Ding, H. Zhang, M. Lin, and J. Wang, "Joint optimization of transmission bandwidth allocation and data compression for mobile-edge computing systems," *IEEE Communications Letters*, vol. 24, no. 10, pp. 2245–2249, Oct. 2020.
- [9] Q. Tang, Z. Fei, B. Li, and Z. Han, "Computation offloading in LEO satellite networks with hybrid cloud and edge computing," *IEEE Internet of Things Journal*, vol. 8, no. 11, pp. 9164–9176, 2021.
- [10] C. Qiu, H. Yao, F. R. Yu, F. Xu, and C. Zhao, "Deep Q-learning aided networking, caching, and computing resources allocation in software-defined satellite-terrestrial networks," *IEEE Transactions on Vehicular Technology*, vol. 68, no. 6, pp. 5871–5883, 2019.
- [11] N. Cheng, F. Lyu, W. Quan, C. Zhou, H. He, W. Shi, and X. Shen, "Space/aerial-assisted computing offloading for IoT applications: A learning-based approach," *IEEE Journal on Selected Areas in Communications*, vol. 37, no. 5, pp. 1117–1129, 2019.

- [12] A. Alsharoa and M.-S. Alouini, "Improvement of the global connectivity using integrated satellite-airborne-terrestrial networks with resource optimization," *IEEE Transactions on Wireless Communications*, vol. 19, no. 8, pp. 5088–5100, 2020.
- [13] J. Liu, X. Du, J. Cui, M. Pan, and D. Wei, "Task-oriented intelligent networking architecture for the space–air–ground–aqua integrated network," *IEEE Internet of Things Journal*, vol. 7, no. 6, pp. 5345–5358, 2020.
- [14] X. Li, C. You, S. Andreev, Y. Gong, and K. Huang, "Wirelessly powered crowd sensing: Joint power transfer, sensing, compression, and transmission," *IEEE Journal on Selected Areas in Communications*, vol. 37, no. 2, pp. 391–406, 2019.
- [15] "Digital Video Broadcasting (DVB); Second generation framing structure, channel coding and modulation systems for broadcasting, interactive services, news gathering and other broadband satellite applications (DVB-S2)," ETSI, France, Standard, October 2014.
- [16] K. Cheng, Y. Teng, W. Sun, A. Liu, and X. Wang, "Energy-efficient joint offloading and wireless resource allocation strategy in multi-MEC server systems," in *Proc. IEEE International Conference on Communications (ICC)*, 2018.
- [17] W. Zhang, Y. Wen, K. Guan, D. Kilper, H. Luo, and D. O. Wu, "Energy-optimal mobile cloud computing under stochastic wireless channel," *IEEE Transactions on Wireless Communications*, vol. 12, no. 9, pp. 4569–4581, 2013.
- [18] Y. Mao, C. You, J. Zhang, K. Huang, and K. B. Letaief, "A survey on mobile edge computing: The communication perspective," *IEEE Communications Surveys & Tutorials*, vol. 19, pp. 2322–2358, 10 2017.
- [19] B. Matthiesen, A. Zappone, K. L. Besser, E. A. Jorswieck, and M. Debbah, "A globally optimal energy-efficient power control framework and its efficient implementation in wireless interference networks," *IEEE Transactions on Signal Processing*, vol. 68, pp. 3887–3902, 2020.
- [20] P. Tseng, "Convergence of a block coordinate descent method for nondifferentiable minimization," *Journal of Optimization Theory and Applications*, vol. 109, pp. 475–494, 2001.
- [21] D. P. Bertsekas, "Multiplier methods: A survey," *Automatica*, vol. 12, pp. 133–145, 3 1976. [Online]. Available: <https://linkinghub.elsevier.com/retrieve/pii/0005109876900777>
- [22] Q. Shi and M. Hong, "Penalty dual decomposition method for nonsmooth nonconvex optimization—part i: Algorithms and convergence analysis," *IEEE Transactions on Signal Processing*, vol. 68, pp. 4108–4122, 2020.
- [23] S. Diamond and S. Boyd, "CVXPY: A Python-embedded modeling language for convex optimization," *Journal of Machine Learning Research*, vol. 17, no. 83, pp. 1–5, 2016.
- [24] S. Boyd and L. Vandenberghe, *Convex Optimization*, 7th ed. New York: Cambridge University Press, 2009.